Thermoelectric properties of ZnO ceramics densified through spark plasma sintering

P M Radingoana, Sophie Guillemet-Fritsch, J Noudem, P A Olubambi, G Chevallier, C Estournès

Microstructure and Thermoelectric Properties of Al-doped ZnO ceramic prepared by Spark Plasma Sintering

P.M. Radingoana[1,4], S. Guillemet-Fritsch[1,*], J. Noudem[2], P.A. Olubambi[3], G. Chevallier[1], C. Estournès[1]

[1]*CIRIMAT, Université de Toulouse, CNRS, Université Toulouse 3 - Paul Sabatier, 118 Route de Narbonne, 31062 Toulouse cedex 9 - France.*
[2]*Normandie Univ, Ensicaen, Unicaen, CNRS, CRISMAT, 14000 Caen, France*
[3]*University of Johannesburg, School of Mining, Metallurgy and Chemical Engineering, Johannesburg, South Africa*
[4]*Advanced Materials Manufacturing, Manufacturing Cluster, Council for Scientific and Industrial Research, P.O. Box 395, Pretoria, 0001, South Africa*

***Corresponding author:** Sophie Guillemet-Fritsch: sophie.guillemet@univ-tlse3.fr

Abstract

The high thermal and low electrical conductivity of ZnO ceramics have hindered their thermoelectric applications. The doping of ZnO with group 3 elements can enhance the thermoelectric properties. In this work, Al (2at %) doped ZnO powder was sintered using spark plasma sintering at varying parameters (such as temperature (550-700 °C), pressure (250-500 MPa) and the point of pressure application (Room temperature (RT) and holding time (HT))). Maximum relative density of 98.9% was achieved at a temperature and pressure of 650°C and 250 MPa, respectively. The Al-doped ZnO ceramics improved in electrical conductivity which caused a decrease in the Seebeck coefficient because of increased carrier concentration. The reduction in the grain size due to inhibiting growth effects of aluminum lead to a decrease in the thermal conductivity through phonon scattering at the grain boundaries. Hence, ZT of $1.5x10^{-3}$ at 500°C was obtained. This study indicated that Al-doped ZnO ceramics can be sintered at very low temperature of 650°C, this helps to retain the nanostructure which is beneficial in improving the thermoelectric properties.

Keywords: ZnO, Aluminum, Thermoelectric properties, Spark plasma sintering, Ceramics

1. Introduction

Over the years, there has been a great progress in the thermoelectric performance of n-type ZnO based ceramics (such as Group 3 elements doping, polymer insertion, morphology modification etc.…) [1-8]. We recently reported on the thermoelectric properties of pure zinc oxide (ZnO) [9]. According to the literature, doping ZnO with group 3 elements (such as aluminum (Al), gallium (Ga), indium (In)) can lead to enhanced electrical properties because dopants can modify the band gap of the oxide. Furthermore, their ionic radius are close to that of Zn (Al^{3+}=0.054 nm, In^{3+}= 0.08 nm, Ga^{3+}= 0.062 nm, Zn^{2+}= 0.074 nm) [10, 11]. Therefore, the ZnO structure will remain the same and the doping may generate free electrons in the conduction band.

Thus far, the highest ZT reported for doped ZnO ceramics is from dual doping of Al and Ga; ZT = 0.45@1000 K and ZT = 0.65@1247 K obtained using conventional sintering [12]. Al-doped ZnO ceramics were extensively investigated with ZTs of ~ 0.17 to 0.47 at 1000 K from ceramics prepared through hot press [12-15], microwave [16] and spark plasma sintering [17-22]. The substitution of Al on the zinc site of ZnO helps to improve thermoelectric properties through enhanced electrical conductivity and reduced thermal conductivity caused by nanostructuring. Aluminum is known to be a grain growth inhibitor [23, 24].

However, these properties can be easily affected by the preparation methods of the doped powders. In most reported works, the authors have prepared them by solid state reactions of ZnO and Al_2O_3 raw powders which can cause inhomogeneity in the material [25]. The most reliable technique is the synthesis of the powders by wet chemical methods that lead to a homogenous mixture [26, 27]. Nowadays, consolidation is being conducted using spark plasma sintering (SPS) technique; resulting in full densification which is attained in a short period which minimizes grain growth [28, 29]. Smaller grains are effective for reducing thermal conductivity through phonon scattering [30, 31] and increasing the Seebeck Coefficient [16, 32]. So, bulk materials with smaller grains provide the most promising thermoelectric properties. Thus, it is important to develop various grain size manipulation techniques to obtain improved thermoelectric properties.

Recently, cold sintering process (CSP) [33-36] and functional graded material (FGM) [37, 38] are reported to control the grain size of bulk materials. Cold sintering process adds small fraction of aqueous solution into powder to assist with densification of ceramics at very low temperatures of ~200℃, as a result, the nanostructure of the material is maintained [36]. Whereas FGM improves the efficiency and temperature range of TE materials through continuous grain size gradient [37]. FGM Al-doped ZnO (0-5 wt% Al) layered ceramic prepared using spark plasma sintering at 1000℃ indicated that the current density could be widened which provides temperature range of useful energy conversion [38]. However, impurity phase, $ZnAl_2O_4$, was observed in the ceramic which has a huge impact on the resistivity. This is in accordance with other reported work on Al-doped ZnO ceramics prepared by spark plasma sintering, the presence of spinel phase is problematic [17, 19, 20, 22]. So, obtaining lesser spinel phase is desirable for better electrical conductivity.

During spark plasma sintering the thermal distribution is determined by the current density that has a great influence on the grain size, concentration of impurity phases (e.g $ZnAl_2O_4$) and dislocation defects [39-41]. For instance, sintering with high current density in Al-doped ZnO ceramics contributes to refined grain size and enhanced concentration of impurity phase, $ZnAl_2O_4$ [39]. Chen et al. [42] reported that sintering in low oxygen partial pressure leads to better substitution of Al ions into the ZnO lattice as compared to high oxygen partial pressure where it is transformed into spinel phase. Therefore, great caution needs to be taken when setting sintering conditions (such as temperature, current density, pressure, atmosphere etc.) for spark plasma sintering of Al-doped ZnO ceramics. This will assist to have a better understanding of the influence of spark plasma sintering parameters on the microstructure and thermoelectric properties of these ceramics.

In this present work, ZnO was doped with 2 *mol%* Al because of the previously reported high ZT of between 0.3 – 0.45 at temperatures of about 1000K due to high electrical conductivity and reduced thermal conductivity [12, 19, 22]. The $Zn_{0.98}Al_{0.02}O$ powder was synthesized through co-precipitation followed by calcination. The sintering was performed using Spark plasma Sintering (SPS) at varying temperatures, pressures and point of pressure application to find full densification and suitable microstructure (i.e. fully densified with as much as possible low grain size). This discussion includes characterization of bulk samples, densification characteristics and thermoelectric properties of the Al-doped ZnO polycrystalline materials.

2. Materials and methodology

2.1 Materials

Al (2at%) doped ZnO powder was synthesized through the wet chemical method. Basically, the co-precipitation techniques followed by calcination, similarly to the procedures previously developed by Guy *et al.* [43, 44].

2.2 Spark plasma sintering of the $Zn_{0.98}Al_{0.02}O$ powder

Al-doped ZnO powders were densified under air atmosphere with a Dr. Sinter 2080 unit (SPS Syntex Inc., Japan) available at the Plateforme Nationale de Frittage Flash (PNF2) located at the Université Toulouse 3 Paul Sabatier using tungsten carbide molds with 8 and 20 mm inner diameters. Prior to their filling with the powder, the molds were lined with 0.2 mm thick graphite foil (PERMAFOIL®Toyo Tanso). A pre-compaction step at 25 MPa for 1 min was systematically applied before the thermal cycle to ensure the same initial green state for all the samples. The influence of sintering temperature (550-700°C), pressure (250-500 MPa) and point of applied pressure (room temperature (RT) or at the setpoint temperature (HT-Holding Temperature) was investigated. The sintered ceramics were polished by silicon carbide discs (P320 and P600) to remove graphite foil for further characterizations.

2.3 Characterization techniques

Dense ceramics

The particle size and the morphology of the starting powders and the microstructure of the dense ceramics were investigated using Scanning Electron Microscopy (MEB JEOL JSM65 10LV). X-ray diffractometer (XRD Bruker D4) was used to analyse the phase structure. The surface area and particle size distribution were conducted using Brunauer–Emmett–Teller technique (BET) (Micromeritics desorb 2300A) and the mastersizer (Mastersizer 2000 (CRISMAT) and Mastersizer 3000 (CIRIMAT)), respectively.

Electrical properties

The electrical measurements were conducted at the Laboratoire de Cristallographie et Sciences des Matériaux (CRISMAT, UMR 6508 CNRS, CAEN France). Seebeck coefficient and resistivity of the dense ceramics were simultaneously measured using ZEM-3 (Ulvac-Riko) in argon atmosphere. The dense ceramics were cut into 9x3x3 mm bars and coated with gold to ensure electrical ohmic contact. Graphite foil was inserted on both sides of

heaters to have a good electrical and thermal contact with the sample. The thermal conductivity was determined by measuring separately thermal diffusivity (α), ceramic density (d) and heat capacity (Cp) (Eq.01). The samples were cut to dimensions of 6x6x1 mm.

$$k = \alpha(T)\mathrm{Cp(T)d(T)} \qquad [1]$$

The band gap was determined on ceramics, of diameter 20 mm and thickness 0.5 mm, through the photovoltaic route using Bentham PVE 300 PV. The Hall Effect measurements were performed on 3x3 mm square samples using a commercial physical property measurement system (Model 7100 AC transport controller, Quantum Design).

3. Results and discussion

3.1 Spark plasma sintering of Al-doped ZnO powder

The Al-doped ZnO powder ($Zn_{0.98}Al_{0.02}O$) was sintered by SPS in air at various parameters such as temperature, pressure and point of pressure application in order to get fully dense ceramics. Indeed, it has been previously shown that the use of WC tools allows to process oxide materials by SPS under air atmosphere and to overcome the problem of reduction due to the low oxygen partial pressure (neutral atmosphere, graphitic environment or dynamic vacuum) commonly encountered [45, 46]. As a consequence, the annealing treatment, usually performed around 800°C, is not necessary to re-oxidized the specimen which can induce grain growth. The summary of the ceramics characteristics for different sintering conditions are given in Table 1.

3.1.1 Sintering behavior of Al-doped ZnO ceramics

The shrinkage curves of the pure ZnO and the *2 at%* Al doped powders are given in Fig. 1. The shrinkage of both samples increased sharply till 550°C. The sintering steps of *2 at%* Al-doped ZnO can be divided into three segments; the first stage is the rearrangement of the nanoparticles due to applied pressure. The displacement of *2 at%* was slow and reached only 0.7 mm as compared to 1.2 mm for *0 at%*, could be related to the aggregates present in the powder. The second stage is related to the progressive breaking of the remaining agglomerates and/or to the neck formations between the particles due to localized heating caused by spark discharge [26, 28, 47, 48]. The third stage is related to extend of the neck's formation between the particles and to the densification step with progressive pore elimination. After 550°C, the slight increase in displacement of both samples could be due to final densification with elimination of the residual pores [49]. The total displacement between these samples differed by 0.5mm. This difference can be related to the influences of grain size on the sintering behavior of the ceramics. The higher density of grain boundaries in the doped sample compared with the pure ZnO could have enhanced the diffusion rate [50], as visible in zone 2 where the kinetics are higher. As a result, the optimal sintering temperature decreased. The reduction in the sintering temperature has been reported on the sintering of nanoparticles materials such as ZnO [28, 51]. Reduced temperature implies less grain growth and more grains boundaries, which will be beneficial for improving thermoelectric properties. The relative densities of the ceramics are given in Table 4 from sintering temperature of 550°C to 700°C.

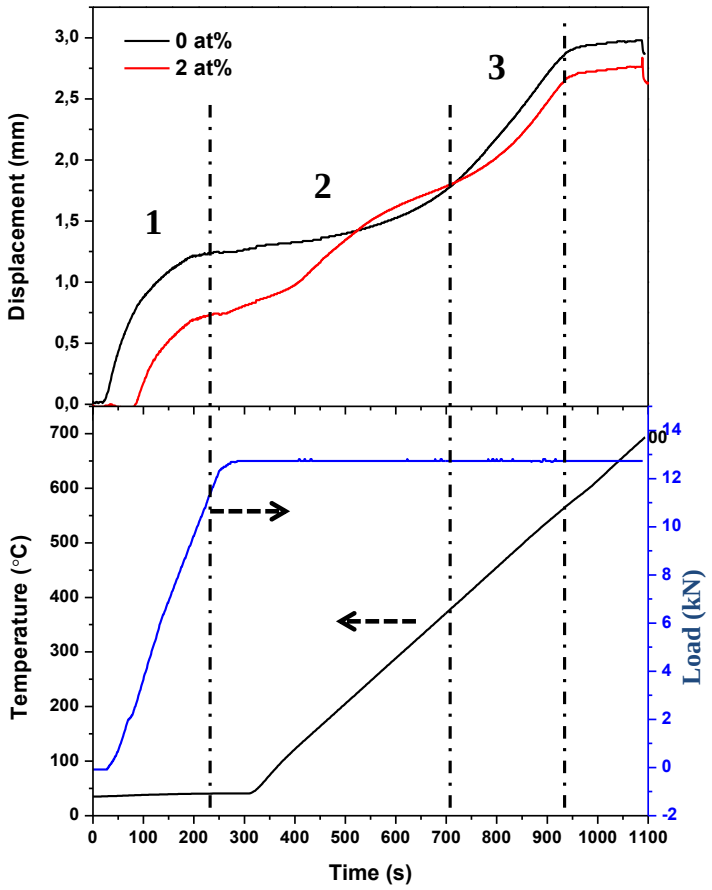

Fig.1 Sintering behavior of pure ZnO and Al-doped ZnO using spark plasma sintering

Table 1 Summary of pure and Al-doped ZnO ceramics characteristics for varied SPS parameters (*Note: RT-Room temperature, HT- Holding time*)

Ref.	Temperature	Initial Pressure	Final Pressure	Point of Pressure application	Atmosphere	RD	Grain size
	°C	MPa	MPa	°C		%	µm
ZnO							
1	600	25	250	RT	Air	99.3±0.1	2.4±0.6
2	700	25	250	RT	Air	100	5±2
$Zn_{0.98}Al_{0.02}O$							
3	RT	250	250	RT	Air	57±0.2	-
4	550	250	250	RT	Air	79.9±0.5	-
5	600	250	250	RT	Air	84.9±0.2	-
6	650	250	250	RT	Air	98.9±0.1	0.46±0.01
7	700	25	250	RT	Air	98.1±0.1	0.76±0.26
8	600	25	250	HT	Air	84.3±0.2	-
9	650	25	250	HT	Air	98.6±0.1	0.09±0.02
10	600	100	500	HT	Air	98.5±0.1	-
[$Zn_{0.98}Al_{0.02}O$] Bibliography							
Ma *et al.* [52]	900	50	50	-	Vacuum	99.9	-
Nam *et al.* [19]	900	50	50	-	Vacuum	94	0.2
Han *et al.*[18]	950	50	50	-	Vacuum	90	-

3.1.2 Effect of sintering temperatures

The influence of the sintering temperature between 550-700°C on the structure, the microstructure, and the density of Al-doped ZnO ceramics was studied. Relative density versus temperature given in Fig. 2 showed an increase in the relative density with an increment in the temperature. Maximum relative density of 98.9% was achieved at 650°C, with initial relative green density of 57% at room temperature. Beyond 650°C a decrease in the relative density was observed which could be due to the presence of pores and/or decrease in the ceramic density related to the physical properties such as the density of the individual materials [52, 53]. For instance, at 700°C the concentration of secondary phases increases, see XRD, which have lesser density as compared to that of ZnO. The sum of the total density of the ceramic will drop. Ma et al. [52] reported higher densification rate (i.e. 99.9%) but such level was obtained after sintering in reduced atmosphere for higher sintering temperature (i.e. 900°C) than the range explored in the present study. While, Nam *et al.* [19] and Han et al. [18] found lower relative densities of 94% and 90% at temperatures of 900°C and 950°C, respectively, by sintering in vacuum. Other reports mentioned relative densities of 99% at temperatures between 800-1200°C and only 65-93% sintering between 700-900°C for Al-doped ZnO ceramics [17, 54]. In the present study we want to point out that a high relative density of 98.9% was obtained at a temperature of only 650°C and high pressure of 250 MPa. The achievement of such high relative density at low temperature could be due to the combination of high reactivity of the powders (i.e. small grain size), better rearrangement of the grains, and higher pressure applied.

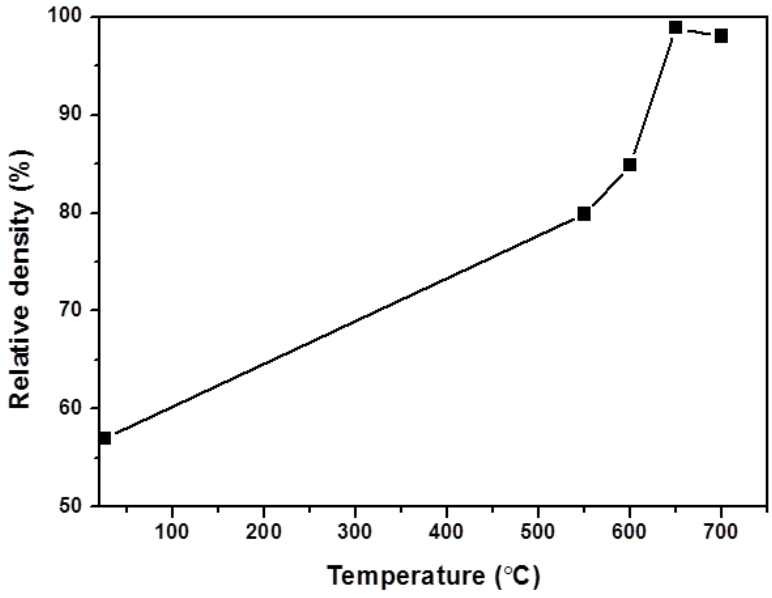

Fig.2 Relative density versus temperature of Al-doped ZnO ceramics

The analysis of the XRD patterns of most of the Al-doped ZnO ceramics (Fig.3) showed that the main phase corresponds to the ZnO hexagonal Wurzite structure. It was observed that as the sintering temperature increases the XRD peaks of the ceramics are sharpened which is related to the increase in the grain size. The zoomed inserted image indicated the presence of

spinel phase ($ZnAl_2O_4$) with very small peaks at 37°, 35°, 32.5° and 31.5°. This indicates that sintering at low temperatures in air there is efficient incorporation of Al ions in ZnO lattice as compared to at high temperatures where it is transformed into a spinel phase. This is because of the differences in the partial pressure of oxygen, the lower the temperature the lower the partial pressure of oxygen in the air and vice versa, see Fig.4 [42, 55]. Low partial pressure of oxygen promotes further substitution of Al into the ZnO structure. Whereas, in high oxygen partial pressures excess Al reacts with ZnO to form $ZnAl_2O_4$. This is in line with reported work on the comparison between conventional and SPS of Al-doped ZnO ceramics sintered at 1200℃ in air and 1000℃ in vacuum, respectively [42]. It was found that the samples exposed to air had high concentration of spinel phase compared to those in vacuum due to the differences in oxygen partial pressure and rapid dissolution of Al ions into ZnO lattice caused by the high DC current applied in SPS process. Similarly, high concentration of spinel phase was observed in air than in nitrogen atmosphere prepared using conventional route at 1400℃ for Al-doped ZnO ceramic[56]. Nunes and Bradt [57] report on conventionally sintered $ZnO/Bi_2O_3/Al_2O_3$ ceramics found that the majority of the activation energy (400 kJ/mol) was related to the transport of the $ZnAl_2O_4$ spinel particles which are most probably controlled by the diffusion of 0^{2-} ions in the $ZnAl_2O_4$ spinel structure.

It is possible that this secondary phase present in higher quantity at higher temperature could have contributed to the decrease in the relative density at 700°C, the density of $ZnAl_2O_4$ phase is 4.61 g/cm^3, compared to ZnO (i.e. 5.61g/cm^3).

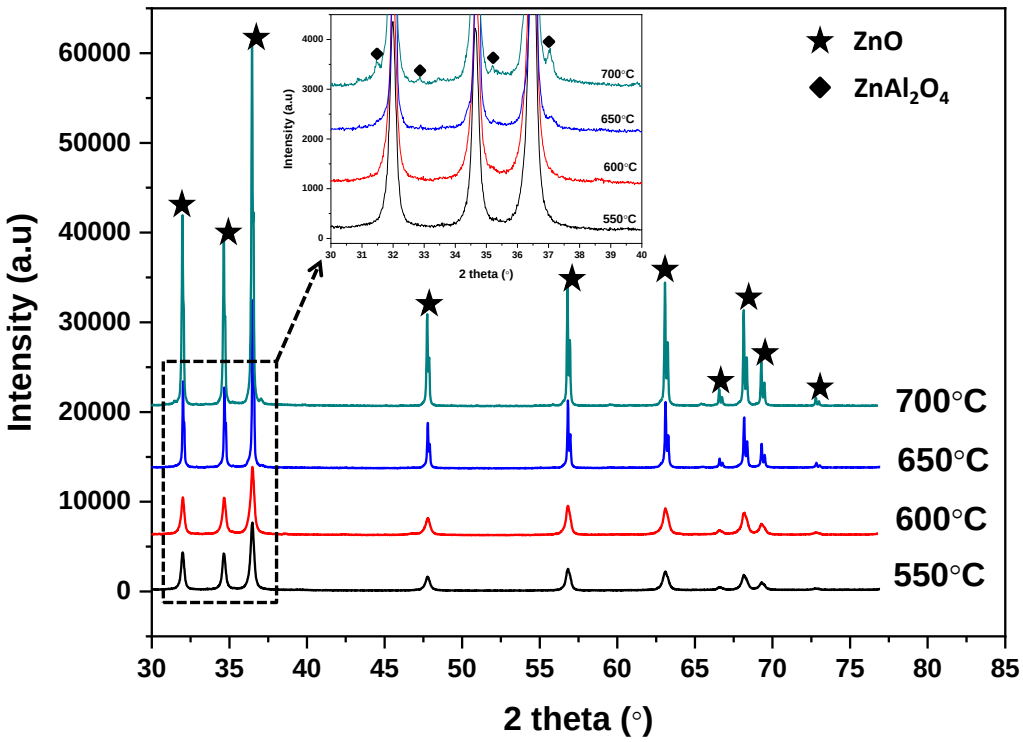

Fig.3 XRD patterns of Al-doped ZnO ceramics at varying temperature

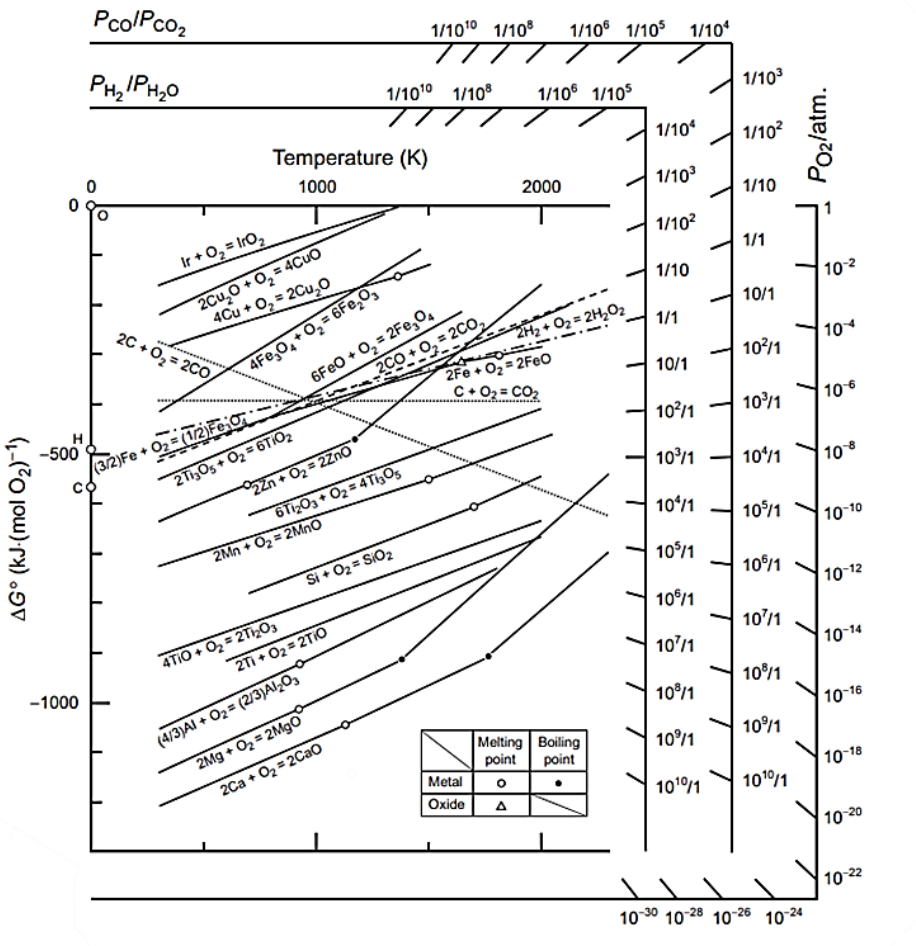

Fig.4 Ellingham diagram of some metal oxides [58]

The SEM micrograph of *0 at%* and 2 at% Al doped ZnO ceramics sintered at 700°C are given in Fig. 5. It is shown that there is a decrease in the grain size when 2 at% Al is doped in the ZnO from 5.8 µm (0 *at%)* to 0.76 µm (2 *at%*) (see Fig. 5 (a) and (b)). This could be due to the grain growth inhibiting effects of aluminum as discussed in previous sections. Further studies were done to understand the influence of sintering temperature on the microstructure of 2 at% Al doped ZnO. It was observed that sintering at 550°C and 600°C did not change the grain size of the ceramics. However, at a temperature of 650°C and 700°C the grain size increased from initial grain size of 75 nm to 457 nm and 760 nm, respectively, (see Fig. 5 ((b) and (c)). EDX analysis on the sample sintered at 700°C indicated that the light phase is Al rich and the dark phase is Zn rich. This can be supported by the XRD results because the $ZnAl_2O_4$ is Al rich phase. Therefore, the light phase in the SEM analysis is the spinel phase of $ZnAl_2O_4$ as determined by the XRD analysis. This is in conformity with the $ZnAl_2O_4$ peak observed in XRD by Jood *et al.* [16]. It was noticed on their SEM observations that the spinel phase is homogeneously distributed across the sample. The presence of the spinel phase will influence the electrical properties such as resistivity and carrier mobility. Some reports indicated that it could lead to a decrease of the thermal conductivity while on the other hand it could be a hindrance in improving the electrical conductivity due to electron scattering [13, 16-19, 25]. EDS analysis of the sample sintered at 650°C did not indicate any secondary phases which may be attributed to the low concentration of $ZnAl_2O_4$. Further studies were

conducted to reduce the concentration of secondary phase in the ceramics while keeping high densification.

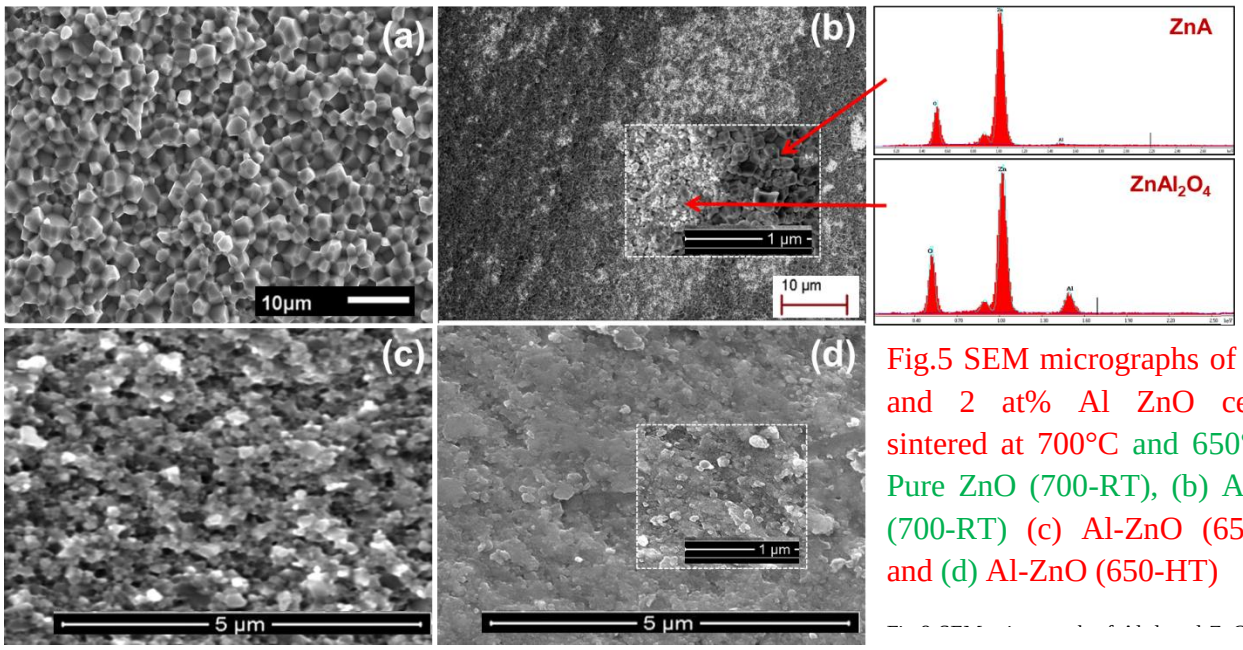

Fig.5 SEM micrographs of 0 at% and 2 at% Al ZnO ceramic sintered at 700°C and 650°C (a) Pure ZnO (700-RT), (b) Al-ZnO (700-RT) (c) Al-ZnO (650-RT) and (d) Al-ZnO (650-HT)

3.1.3 Reduction of the amount of spinel phase in Al-doped ZnO ceramics

In the previous section, it was indicated that sintering at temperature above 650°C with a pressure of 250 MPa applied at room temperature causes the formation of the secondary phases that can be a hindrance in improving thermoelectric properties. One way to avoid the presence of spinel phase in the sintered ceramics is to decrease the setpoint temperature below 650°C while conserving the objective to obtain dense specimen. To do so two strategies have been followed: the first one is to apply the high pressure at the holding point/temperature (HT) and the second one is to double the pressure. At first the influence of the changes in sintering conditions on the densification was determined. For a set point temperature of 600°C, the relative densities of the samples reached only 84% even though a pressure of 250 MPa is applied at room temperature and at the dwell (HT), see Table 1. An increase in the relative density from 84 to 98.5% was observed when the sintering pressure was increased to 500 MPa during heating stage at a temperature of 600°C. However, the sintered ceramic cracked at this pressure due to distribution of residual stresses during cooling of sintered ceramic [59]. So, an optimal densification of 98.6% was achieved at 650°C and 250 MPa without cracks. This will be beneficial in improving the electrical conductivity and better thermoelectric properties.

The XRD patterns of the ceramics sintered at different temperatures and point of applied pressure are reported in Fig. 6. For all the samples, the major phase present is ZnO with the same hexagonal structure of the powder. It is presented that applying pressure during the dwell time (HT) for both 600°C and 650°C, the secondary phases were not detected as

compared to applying the pressure at room temperature (RT). This could be due to the rapid diffusion of Al atoms which promotes the replacement Al ions into the ZnO lattice [42].

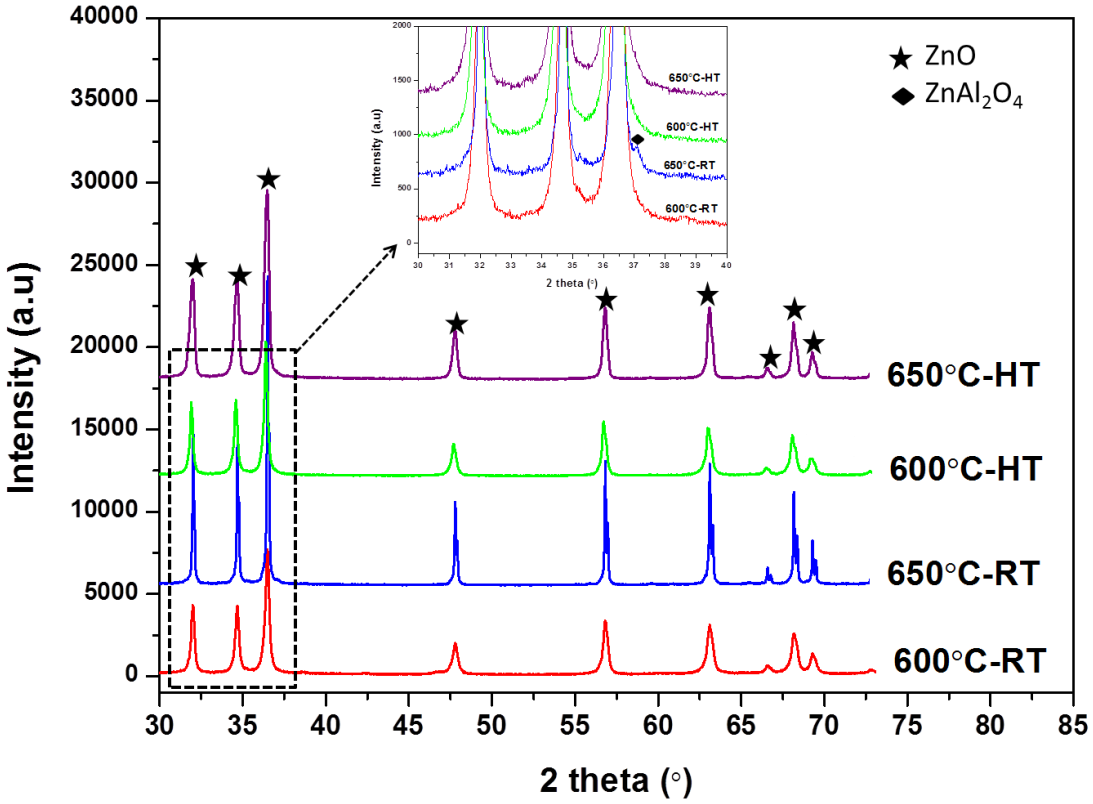

Fig.6 XRD patterns of Al-doped ZnO ceramics sintered at 600°C and 650°C with a pressure of 250 MPa using RT and HT mode

SEM micrograph of the sample sintered at 650°C using HT mode (Fig.5 (d)) revealed that the nanostructure of the sample is maintained compared to the sample sintered using RT mode. The differences in heat transfer between the grains could have caused the grain size difference; RT mode had better contact as compared to HT mode [48]. This polycrystalline sample was further annealed in air at 600°C for 24 h (not shown) to obtain fully oxidized ceramic to ensure stable measurement and reproducibility of electrical properties. XRD analysis of the annealed sample did not show any changes in the phase structure and the grain size slightly increased from 90 nm to 140 nm.

3.2 Thermoelectric properties

The thermoelectric properties were determined for the annealed ceramic sintered at 650°C (HT) as it contains minimal/no secondary phase and exhibit a densification rate of 98.6%. see Fig 7. The resistivity as a function of temperature is given in Fig. 7 (a); for the samples *0 at%* and *2 at%*. It is shown that addition of Al in ZnO reduces the resistivity especially at low temperature (< 200°C). At 50°C the resistivity reduced from ~1960 Ω.cm to ~50 Ω.cm for *0 Al at%* and 2 Al *at%*, respectively. This difference is attributed to the substitution of Al^{3+} ions on the Zn^{2+} site creating extra free electrons [17-22]. It is observed that the resistivity of both

samples decreases with an increase in temperature, which is significant of a semiconducting behavior. At high temperature the valence electrons gain enough energy to reach the conduction band, hence, the lowest resistivity of about 1 Ω.cm at 500°C [60]. Sondergaard *et al.*[61] reported a lower resistivity compared to our samples for the same Al content, i.e. resistivity values of 0.005 and 0.0015 Ω.cm at room temperature were obtained for samples sintered at 850°C and 900°C, respectively, using spark plasma sintering in vacuum. This difference is probably due to high carrier concentration caused by differences in preparation methods and particularly the annealing treatment after sintering. Sondergaard *et al.*[61] performed an annealing treatment in air for a week at 800 °C while in our case , the treatment was chosen at much lower temperature, to avoid the grain growth, i.e. 600 °C (because of our low sintering temperature) for 24 h in air also. Obviously, the annealing at 800 °C for such a long time leads to the creation of more oxygen vacancies that significantly reduce the resistivity.

The Seebeck Coefficient as a function of temperature is given in Fig. 7 (b). The negative sign indicates and confirms the *n-type* conductivity. Adding 2 *at%* Al reduced the Seebeck coefficient value from 800 to 175 µV/K at 50°C. This decrease could be caused by the increase in the carrier concentration. The broadband equation (1) indicates inverse relationship between Seebeck coefficient and carrier concentration [62].

$$S_{bulk} = \frac{8m^*\pi^2 k_b^2}{3eh^2} T \left(\frac{\pi}{3n}\right)^{\frac{2}{3}} \quad (1)$$

The absolute Seebeck Coefficient, |S|, for the *2 Al at%* sample increases with an increase in temperature from 50°C to 500°C; which is related to the scattering of the electrons at high temperature. The behaviour is different from pure ZnO which showed a decrease in the |S| with temperature increment. Sondergaard *et al.*[61] reported similar behaviour to that of 2at% Al-doped ZnO with |S| of about 125 µV/K at 50°C for sintering at 850°C and 900°C.

The temperature dependence of the thermal conductivity of the polycrystalline ceramic presented in Fig. 7 (c) revealed that doping with Al into ZnO ceramic reduces the thermal conductivity from 50 W/m.K (0at%) to 27 W/m.K (2at%) at 50°C. This was caused by phonon scattering at the grain boundaries because of reduced grain size [17-22]. It is clearly shown that the thermal conductivity determined in this present work is almost similar to that reported by Sondergaard *et al.*[61] probably because of similar grain size. A grain size difference of only 20nm was determined between the present study and that of Sondergaard *et al.* [61].

The performance of the ceramics was determined using figure of merit, ZT, given in Fig. 7 (d). An increase in ZT was observed with temperature increment for all samples. It was observed that *0 at%* performs better than the *2 at%* ceramic by a ZT value of 1.5×10^{-3} at a temperature of 500°C. The improved performance is because of high Seebeck Coefficient shown by *0 at%* ceramics. The performance of the *2 at%* can be enhanced by improving the solubility of Al in ZnO through process manipulations such as sintering temperature increment and operating in vacuum to increase the electrical conductivity. Also, new

materials could be incorporated with the Al-doped ZnO ceramic to enhance the electrical conductivity while maintaining the nanostructure of ceramic.

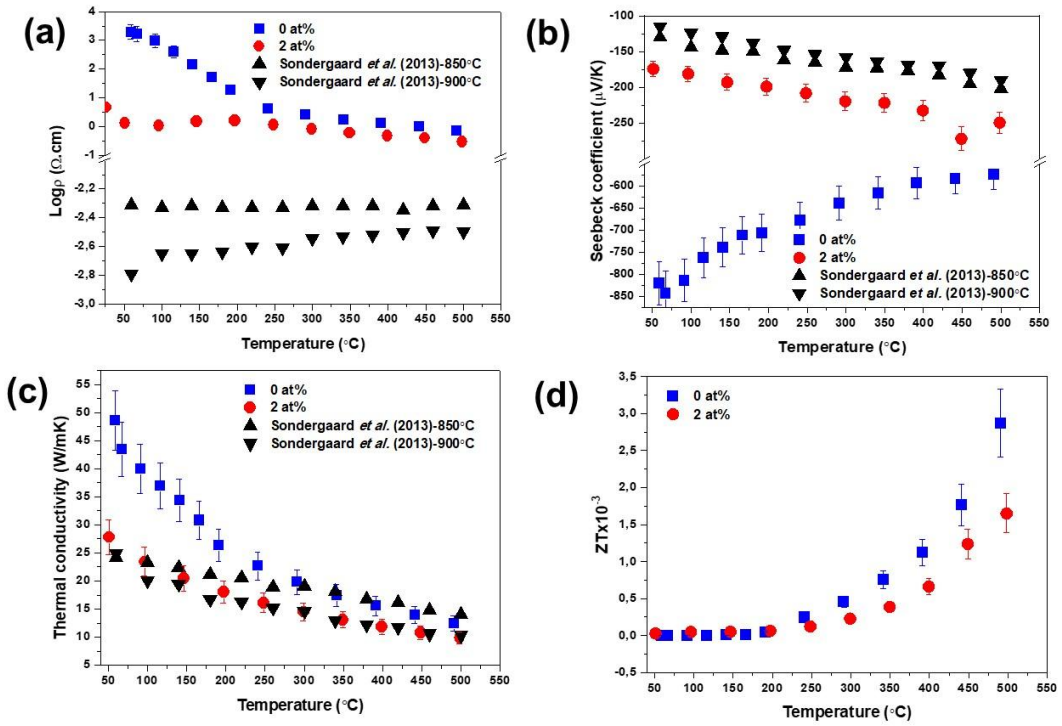

Fig.7 Thermoelectric properties of annealed pure and Al-doped ZnO ceremicc sintered at 650°C (HT): (a) Resistivity (b) Seebeck Coefficient (b) Thermal conductivity (d) Figure of merit (ZT)

4. Conclusions

The synthesis and spark plasma sintering of Al-doped ZnO powder was described. The addition of 2 at% Al in ZnO powder reduces the grain size from 177 to 75 nm. The relative density of Al-doped ZnO sintered at a temperature of 650°C reaches high relative density of 98.9%. Sintering above 650°C causes an increase in the grain size which consequently decreases the relative density due to pores. The addition of Al into the ZnO ceramics caused a decrease in the grain size from 5.4 μm (without Al) to <1 μm (with 2 at% Al). Sintering above 650°C and applying the axial pressure during room temperature causes the presence of spinel phase, $ZnAl_2O_4$, which is unwanted for thermoelectric properties. Applying the pressure during holding time prevents the formation of spinel phase. The concentration of spinel phase is influenced by the oxygen partial pressure. The resistivity of the Al-doped ZnO ceramics slightly reduces, which causes a decrease in the absolute Seebeck Coefficient as a result of increased carrier concentration. The reduction in the grain size leads to a decrease in the thermal conductivity due to phonon scattering at the grain boundaries. As a result, ZT value of $1.5x10^{-3}$ at 500°C, smaller than the one of pure ZnO ceramics was obtained. The low Seebeck Coefficient and electrical conductivity value of Al-doped ZnO ceramic caused the decrease in the performance. Even so, these results revealed the importance of reduced thermal conductivity and low resistivity to improve the thermoelectric properties of Al-doped

ZnO ceramics. It is advised to do further experiments to optimize the amount of Al dopants in ZnO ceramics are required to improve thermoelectric properties either by incorporating new materials to develop new composites and/or play with oxygen stoichiometry by optimizing sintering and annealing parameters especially the operating atmosphere.

5. Acknowledgements

This project was funded by A European and South African Partnership on Heritage and Past+ (AESOP+, Europe) (551128-EM-1-2014-1-FR-ERA MUNDUS-EMA21) and National Research Fund (NRF, South Africa) (102699). The authors would like to thank J. Lecourt, F. Veillon and C. Bilot from CRISMAT laboratory for their technical assistance.

6. References

1. Fergus, J.W. *Oxide materials for high temperature thermoelectric energy conversion*. Journal of the European Ceramic Society, 2012. **32**, 525-540 DOI: 10.1016/j.jeurceramsoc.2011.10.007.
2. Feng, Y., et al. *Metal oxides for thermoelectric power generation and beyond*. Advanced Composites and Hybrid Materials, 2017. 1-13 DOI: 10.1007/s42114-017-0011-4.
3. Zhu, B., et al. *Multiple doped ZnO with enhanced thermoelectric properties*. Journal of the European Ceramic Society, 2021. **41**, 4182-4188 DOI: 10.1016/j.jeurceramsoc.2021.01.054.
4. Mitra, M., et al. *Facile synthesis and thermoelectric properties of aluminum doped zinc oxide/polyaniline (AZO/PANI) hybrid*. Synthetic Metals, 2017. **228**, 25-31 DOI: 10.1016/j.synthmet.2017.03.017.
5. Wu, Z.-H., H.-Q. Xie, and Y.-B. Zhai *Enhanced thermoelectric figure of merit in nanostructured ZnO by nanojunction effect*. Applied Physics Letters, 2013. **103**, 243901 DOI: 10.1063/1.4842035.
6. Wu, Y., et al. *Enhanced thermoelectric properties of ZnO: C doping and band gap tuning*. Journal of the European Ceramic Society, 2021. **41**, 1324-1331 DOI: 10.1016/j.jeurceramsoc.2020.09.042.
7. Fedotov, A., et al. *Electron transport and thermoelectric properties of ZnO ceramics doped with Fe*. Journal of Alloys and Compounds, 2021. **854**, 156169 DOI: 10.1016/j.jallcom.2020.156169.
8. Baghdadi, N., et al. *The effect of morphological modification on the thermoelectric properties of ZnO nanomaterials*. Ceramics International, 2021. **47**, 6169-6178 DOI: 10.1016/j.ceramint.2020.10.195.
9. Radingoana, P.M., et al. *Thermoelectric properties of ZnO ceramics densified through spark plasma sintering*. Ceramics International, 2020. **46**, 5229-5238 DOI: 10.1016/j.ceramint.2019.10.271.
10. Jayaraman, V.K., et al. *Effect of co-doping concentration on structural, morphological, optical and electrical properties of aluminium and indium co-doped ZnO thin films deposited by ultrasonic spray pyrolysis*. Materials Science in Semiconductor Processing, 2016. **47**, 32-36.
11. Look, D.C. *Progress in ZnO materials and devices*. Journal of electronic materials, 2006. **35**, 1299-1305.
12. Ohtaki, M., K. Araki, and K. Yamamoto *High thermoelectric performance of dually doped ZnO ceramics*. Journal of Electronic Materials, 2009. **38**, 1234-1238 DOI: 10.1007/s11664-009-0816-1.
13. Tsubota, T., et al. *Thermoelectric properties of Al-doped ZnO as a promising oxide material for high-temperature thermoelectric conversion*. Journal of Materials Chemistry, 1997. **7**, 85-90 DOI: 10.1039/a602506d.

14. Ohtaki, M., et al. *High-temperature thermoelectric properties of (Zn1− x Al x) O*. Journal of applied physics, 1996. **79**, 1816-1818 DOI: 10.1063/1.360976.
15. Fujishiro, Y., et al. *Effect of Microstructural Control on Thermoelectric Properties of Hot-Pressed Aluminum-Doped Zinc Oxide*. Journal of the American Ceramic Society, 2003. **86**, 2063-2066.
16. Jood, P., et al. *Al-doped zinc oxide nanocomposites with enhanced thermoelectric properties*. Nano letters, 2011. **11**, 4337-4342.
17. Gautam, D., et al. *Thermoelectric properties of pulsed current sintered nanocrystalline Al-doped ZnO by chemical vapour synthesis*. Journal of Materials Chemistry A, 2015. **3**, 189-197 DOI: 10.1039/c4ta04355c.
18. Han, L., et al. *Effects of morphology on the thermoelectric properties of Al-doped ZnO*. RSC Advances, 2014. **4**, 12353-12361 DOI: 10.1039/c3ra47617k.
19. Nam, W.H., et al. *High-temperature charge transport and thermoelectric properties of a degenerately Al-doped ZnO nanocomposite*. Journal of Materials Chemistry, 2012. **22**, 14633-14638 DOI: 10.1039/c2jm31763j.
20. Han, L., *High Temperature Thermoelectric Properties of ZnO Based Materials*. 2014, Department of Energy Conversion and Storage, Technical University of Denmark.
21. Han, L., et al. *The influence of α-and γ-Al2O3 phases on the thermoelectric properties of Al-doped ZnO*. Journal of Alloys and Compounds, 2013. **555**, 291-296 DOI: 10.1016/j.jallcom.2012.12.091.
22. Zhang, D.-B., et al. *Hybrid-structured ZnO thermoelectric materials with high carrier mobility and reduced thermal conductivity*. RSC Advances, 2017. **7**, 10855-10864 DOI: 10.1039/c6ra28854e.
23. Zhang, Y., et al. *The Solubility and Temperature Dependence of Resistivity for Aluminum-Doped Zinc Oxide Ceramic*. International Journal of Applied Ceramic Technology, 2012. **9**, 374-381 DOI: 10.1111/j.1744-7402.2011.02666.x.
24. Teranishi, T., et al. *Thermoelectric Property of Polycrystalline Aluminum-Doped Zinc Oxide Enhanced by Micropore Foaming*. Journal of the American Ceramic Society, 2012. **95**, 690-695 DOI: 10.1111/j.1551-2916.2011.04837.x.
25. Cai, K., et al. *Preparation and thermoelectric properties of Al-doped ZnO ceramics*. Materials Science and Engineering: B, 2003. **104**, 45-48 DOI: 10.1016/S0921-5107(03)00280-0.
26. Beynet, Y., et al. *ZnO-based varistors prepared by spark plasma sintering*. Journal of the European Ceramic Society, 2015. **35**, 1199-1208 DOI: 10.1016/j.jeurceramsoc.2014.10.007.
27. Guy, I., *Elaboration and characterization of powders and varistors based on zinc oxide dope*. 1995, Universite Paul Sabatier. p. 201.
28. Chaim, R., et al. *Sintering and densification of nanocrystalline ceramic oxide powders: a review*. Advances in Applied Ceramics, 2008. **107**, 159-169.
29. Guillon, O., et al. *Field-assisted sintering technology/spark plasma sintering: mechanisms, materials, and technology developments*. Advanced Engineering Materials, 2014. **16**, 830-849 DOI: 10.1002/adem.201300409.
30. Holland, M. *Phonon scattering in semiconductors from thermal conductivity studies*. Physical Review, 1964. **134**, A471 DOI: 10.1103/PhysRev.134.A471.
31. Giovannelli, F., et al., *Thermal conductivity and stability of Al-doped ZnO nanostructured ceramics.* Journal of the European Ceramic Society, 2018. **38**(15): p. 5015-5020.
32. Li, J.-F., et al. *High-performance nanostructured thermoelectric materials*. NPG Asia Materials, 2010. **2**, 152.
33. Funahashi, S., et al., *Demonstration of the cold sintering process study for the densification and grain growth of ZnO ceramics.* Journal of the American Ceramic Society, 2017. **100**(2): p. 546-553.

34. Gonzalez-Julian, J., et al. *Unveiling the mechanisms of cold sintering of ZnO at 250° C by varying applied stress and characterizing grain boundaries by Kelvin Probe Force Microscopy*. Acta Materialia, 2018. **144**, 116-128 DOI: 10.1016/j.actamat.2017.10.055.
35. Guo, H., et al. *Cold sintering process: a novel technique for low-temperature ceramic processing of ferroelectrics*. Journal of the American Ceramic Society, 2016. **99**, 3489-3507 DOI: 10.1111/jace.14554.
36. Jiang, X., et al., *Preparation of high density ZnO ceramics by the Cold Sintering Process.* Ceramics International, 2019. **45**(14): p. 17382-17386.
37. Cramer, C.L., et al., *Continuous functionally graded material to improve the thermoelectric properties of ZnO.* Journal of the European Ceramic Society, 2017. **37**(15): p. 4693-4700.
38. Cramer, C.L., et al., *Testing and Modeling of Functionally Graded Aluminum-Doped Zinc Oxide Using Spark Plasma Sintering and Discrete Powder Layers of Varying Composition.* physica status solidi (a), 2022. **219**(1): p. 2100483.
39. Yang, S., et al., *Influence of electric current on microstructure and electrical property of Al-doped ZnO ceramic consolidated by spark plasma sintering.* Ceramics International, 2020. **46**(17): p. 26539-26547.
40. Bagheri, S.M., et al., *Numerical modeling of heat transfer during spark plasma sintering of titanium carbide.* Ceramics International, 2020. **46**(6): p. 7615-7624.
41. Yang, S., et al., *Microstructure and electrical property of aluminum doped zinc oxide ceramics by isolating current under spark plasma sintering.* Journal of the European Ceramic Society, 2016. **36**(8): p. 1953-1959.
42. Chen, H., et al., *Defects and microstructure of highly conducting Al-doped ZnO ceramics obtained via spark plasma sintering.* Journal of the European Ceramic Society, 2020. **40**(15): p. 5529-5534.
43. Guy, I., *Elaboration et caractérisation de poudres et de varistances à base d'oxyde de zinc dopé*. 1995, Toulouse 3.
44. Mory, J.-E., et al., *Poudre d'oxyde de zinc dope, procede de fabrication et ceramique obtenue a partir de ladite poudre*, in *IFI CLAIMS PATENT SERVICES*, P.C.D. FRANCE, Editor. 1993, Jean-Eudes MoryIsabelle GuyDidier SchneiderAbel RoussetRenee LegrosAlain PeigneyPharmacie Centrale De France France.
45. Noudem, J.G., et al., *Thermoelectric properties of Ca0. 9Yb0. 1MnO3− x prepared by spark plasma sintering in air atmosphere.* Scripta Materialia, 2013. **68**(12): p. 949-952.
46. Philippot, G., et al., *Local distortions in nanostructured ferroelectric ceramics through strain tuning.* Advanced Electronic Materials, 2015. **1**(10): p. 1500190.
47. Chaim, R., et al. *Densification and preservation of ceramic nanocrystalline character by spark plasma sintering*. Advances in Applied Ceramics, 2012. **111**, 280-285 DOI: 10.1179/1743676111Y.0000000074.
48. Radingoana, P., et al. *Influence of processing parameters on the densification and the microstructure of pure zinc oxide ceramics prepared by spark plasma sintering*. Ceramics International, 2019. DOI: 10.1016/j.ceramint.2019.02.048.
49. Cavaliere, P., B. Sadeghi, and A. Shabani, *Spark plasma sintering: process fundamentals*, in *Spark plasma sintering of materials*. 2019, Springer. p. 3-20.
50. Ewsuk, K.G., D.T. Ellerby, and C.B. DiAntonio *Analysis of nanocrystalline and microcrystalline ZnO sintering using master sintering curves*. Journal of the American Ceramic Society, 2006. **89**, 2003-2009 DOI: 10.1111/j.1551-2916.2006.00990.x.
51. Dargatz, B., et al. *FAST/SPS sintering of nanocrystalline zinc oxide—Part I: Enhanced densification and formation of hydrogen-related defects in presence of adsorbed water*. Journal of the European Ceramic Society, 2016. **36**, 1207-1220.
52. Ma, N., et al. *Microstructure and thermoelectric properties of Zn1− xAlxO ceramics fabricated by spark plasma sintering*. Journal of Physics and Chemistry of Solids, 2010. **71**, 1344-1349 DOI: 10.1016/j.jpcs.2010.06.006

53. Chaim, R., et al. *Grain growth during spark plasma and flash sintering of ceramic nanoparticles: a review*. Journal of Materials Science, 2018. **53**, 3087-3105.
54. Díaz-Chao, P., et al. *Textured Al-doped ZnO ceramics with isotropic grains*. Journal of the European Ceramic Society, 2014. **34**, 4247-4256 DOI: 10.1016/j.jeurceramsoc.2014.07.009.
55. Imam, M.A., J.S. Young, and R.G. Reddy, *Effect of Oxygen Partial Pressure and Temperature on the Oxidation Behavior of SiB6.* Metallurgical and Materials Transactions B, 2020. **51**(1): p. 386-394.
56. Bérardan, D., C. Byl, and N. Dragoe, *Influence of the preparation conditions on the thermoelectric properties of Al-doped ZnO.* Journal of the American Ceramic Society, 2010. **93**(8): p. 2352-2358.
57. Nunes, S.I. and R.C. Bradt *Grain Growth of ZnO in ZnO-Bl2O3 Ceramics with Ai2O3 Additions*. Journal of the American Ceramic Society, 1995. **78**, 2469-2475 DOI: 10.1111/j.1151-2916.1995.tb08687.x.
58. Hasegawa, M., *Ellingham diagram*, in *Treatise on Process Metallurgy*. 2014, Elsevier. p. 507-516.
59. Tomaszewski, H. *Residual stresses in layered ceramic composites*. Journal of the European Ceramic Society, 1999. **19**, 1329-1331 DOI: 10.1016/S0955-2219(98)00428-2.
60. Pei, Y., et al. *Convergence of electronic bands for high performance bulk thermoelectrics*. Nature, 2011. **473**, 66 DOI: 10.1038/nature09996.
61. Søndergaard, M., et al. *Sintering and annealing effects on ZnO microstructure and thermoelectric properties*. Acta Materialia, 2013. **61**, 3314-3323.
62. Walia, S., et al. *Transition metal oxides–Thermoelectric properties*. Progress in Materials Science, 2013. **58**, 1443-1489 DOI: 10.1016/j.pmatsci.2013.06.003.